Experimental confirmation of transverse focusing and adiabatic damping in a standing wave linear accelerator

S. Reiche,* J. B. Rosenzweig, S. Anderson, P. Frigola, M. Hogan, A. Murokh, C. Pellegrini, L. Serafini,† G. Travish, and A. Tremaine

Department of Physics and Astronomy, University of California, Los Angeles, Los Angeles, California 90095-1547

(Received 28 February 1997)

The measurement of the transverse phase-space map, or transport matrix, of a relativistic electron in a high-gradient, radio-frequency linear accelerator (rf linac) at the UCLA photoinjector is reported. This matrix, which indicates the effects of acceleration (adiabatic damping), first-order transient focusing, and ponderomotive second-order focusing, is measured as a function of both rf field amplitude and phase in the linac. The elements of the matrix, determined by observation of centroid motion at a set of downstream diagnostics due to deflections induced by a set of upstream steering magnets, compare well with previously developed analytical theory [J. Rosenzweig and L. Serafini, Phys. Rev. E **49**, 1599 (1994)]. The determinant of the matrix is obtained, yielding a direct confirmation of trace space adiabatic damping. Implications of these results on beam optics at moderate energy in high-gradient linear accelerators such as rf photoinjectors are discussed. [S1063-651X(97)09508-1]

PACS number(s): 41.75.Ht, 41.85.−p, 29.17.+w, 29.27.Bd

With the rise in use of high-gradient radio-frequency linear accelerators (rf linacs) in devices such as rf photoinjectors [1] and linear collider test facilities [2], there has been increased attention placed on the strong transverse focusing effects present in these devices. These effects, which are due both to first-order transient effects at the entrance and exit of a linac and to second-order ponderomotive (alternating gradient) effects in the body of the periodic linac structure, are of primary importance in understanding the beam transport in moderate energy sections ($5<\gamma=E/m_ec^2<100$) of electron accelerators. While theoretical analyses of the focusing properties of linacs date back to the 1960s [3,4], recent work has produced a more detailed understanding of the ponderomotive force [5] and analytical solutions of these equations for arbitrary acceleration phase and spatial harmonic content of the rf fields have been found [6], which led to a matrix description of the trace space transport.

This matrix treatment of beam dynamics in high-gradient rf linacs, as well as the underlying analytical model for the averaged (over a rf period) transverse forces, has formed the underpinning of much recent work, from the optics of linear collider test facilities [2] to the full theory of space-charge-dominated beam dynamics in rf photoinjectors [7]. While these implementations of the theory have been compared positively with computer simulation, there has been, however, no effort to date, to the authors' knowledge, to verify the theoretical advances with experiment. This paper presents such a verification.

The trace space transport matrix corresponding to a rf linac, which upon multiplication of a transverse trace space vector, e.g. (x,x'), gives the mapping of this vector through the linac, has been derived recently for arbitrary rf phase, amplitude, and spatial harmonic content in the linac. Including all terms to second order in the average accelerating gradient $eE_0\cos(\phi)\equiv\gamma' m_ec^2$, where E_0 is the amplitude of the synchronous ($v_\phi\cong c$) spatial harmonic wave component of the rf field and $\phi=\omega t-kz$ is the phase defined with respect to the maximum acceleration in this wave, the action of a ponderomotive force can be obtained to second order by averaging over the fast alternating gradient first-order forces and the induced lowest-order oscillatory motion, as [5,6]

$$\overline{F_r}=\frac{(qE_0)^2}{8\gamma m_0c^2}\,r\sum_{n=1}^{\infty} b_n^2+b_{-n}^2+2b_nb_{-n}\cos(2\phi)$$
$$\equiv\eta(\phi)\,\frac{(qE_0)^2}{8\gamma m_0c^2}\,r. \tag{1}$$

The coefficients b_n are the Floquet amplitudes of the spatial harmonics, defined by the expression, valid for an ultrarelativistic ($v_b\cong c$) electron,

$$E_z\cong E_0\mathrm{Re}\left[\sum_{n=-\infty}^{\infty} b_n e^{i(2k_0nz+\phi)}\right], \tag{2}$$

where $k_0=\psi/d=\omega/c$ and ψ is the rf phase shift per period of the linac, with $\psi=\pi$ in the structure considered here. The coefficients b_n have been determined for this structure by mapping the on-axis longitudinal profile of the field using a bead frequency perturbation technique. The fundamental ($n=0$) component of the field, with the coefficient normalized to unity, provides the only significant secular (averaged over a period) acceleration, with nearly negligible transverse effects. The other field components, the nonsynchronous spatial harmonics, contribute almost no net secular acceleration, but give rise to second-order focusing through an alternating gradient or ponderomotive effect [5,6]. Typically, forward and backward wave components of the nonsynchronous harmonics have degenerate frequencies in the frame of the rela-

*Permanent address: DESY, Hamburg, Germany.

†Permanent address: INFN-Milano, Milan, Italy.

tivistic electron and therefore interfere, as shown in the form of the terms of the series making up $\eta(\phi)$.

From the averaged force, the differential equation governing the *secular* trajectory of the electron, about which the fast oscillations induced in first order are performed, is derived,

$$x''+\left(\frac{\gamma'}{\gamma}\right)x'+\frac{\eta(\phi)}{8\cos^2(\phi)}\left(\frac{\gamma'}{\gamma}\right)^2 x=0. \tag{3}$$

This linear differential equation is of Cauchy form and its general solutions, given in matrix form, can be found in Ref. [6]. At the ends of a rf structure, there are first-order transient angular kicks associated with entering and exiting the fringing field that are not immediately canceled in first order by a nearby kick. These kicks, again valid when considering the secular trajectory, are given by $\pm\gamma'/2\gamma$ for the exit and entrance regions, respectively. Multiplying the matrices associated with the entrance, interior, and exit of the linac, we have the full trace space transport matrix

$$M=\begin{bmatrix} \cos(\alpha)-\sqrt{\dfrac{2}{\eta(\phi)}}\cos(\phi)\sin(\alpha) & \sqrt{\dfrac{8}{\eta(\phi)}}\dfrac{\gamma_i}{\gamma'}\cos(\phi)\sin(\alpha) \\ -\dfrac{\gamma'}{\gamma_f}\left[\dfrac{\sin(\phi)}{\sqrt{2\,\eta(\phi)}}+\sqrt{\dfrac{\eta(\phi)}{8}}\dfrac{1}{\cos(\phi)}\right]\sin(\alpha) & \dfrac{\gamma_i}{\gamma_f}\left[\cos(\alpha)+\sqrt{\dfrac{2}{\eta(\phi)}}\cos(\phi)\sin(\alpha)\right] \end{bmatrix}. \tag{4}$$

Here

$$\alpha=\left(\frac{\sqrt{\eta(\phi)/8}}{\cos(\phi)}\right)\ln\left[\frac{\gamma_f}{\gamma_i}\right],$$

with γ_i and γ_f the initial and final Lorentz factors of the electron, respectively, which are simply related by $\gamma_f=\gamma_i+\gamma' L$, with L equal to the length of the linac section and $\gamma' m_e c^2$ equal to the averaged (over a period of the linac) acceleration gradient.

An additional condition on the validity of the matrix given in Eq. (4) is that the transport of electrons must be in the region near the axis, so that the transverse fields are given for all significant spatial harmonics by a linear Taylor-series expansion in the radius. This condition can be qualitatively stated by requiring that the beam excursion be small compared to the rf structure iris size.

It should be noted that the matrix M given in Eq. (4) contains information about two distinct physical effects: focusing and adiabatic damping of trace space trajectories. In fact, this matrix can be shown to be factorizable into two matrices [2], one with a unity determinant that displays only a focusing transformation and one that displays only adiabatic damping, i.e., contracts the trace space angle x' by the factor γ_i/γ_f, with this value for the determinant. Thus the determinant of the full matrix M, as can also be verified from Eq. (4), is the ratio of beam energies $\det(M)=\gamma_i/\gamma_f$, expressing exactly, in the limit that $v_b\to c$, the trace space damping associated with acceleration in the linac.

The layout for the present experiments is displayed in Fig. 1. The linac shown here is a component of the UCLA Photoinjector, a rf accelerating section that boosts the energy of a 3.6-MeV photoelectron beam extracted from a high-gradient 1.5 cell π-mode rf gun to approximately 12.8 MeV at maximum in these experiments. This linac is constructed of a novel, high shunt impedance design known as a plane-wave transformer [8] (PWT) and has non-negligible spatial harmonic content [e.g., $\eta(0)=1.23$]. The experimental arrangement is nearly ideal for observing the focusing and adiabatic damping predicted by the matrix given in Eq. (4). This is due to a number of advantages, the first being that the beam can be viewed as essentially pointlike for the purpose of centroid measurements, as it has a short rms phase extent $\sigma_\phi\cong 1°$ (as determined by coherent transition radiation [9] measurements), a low rms normalized emittance, measured as $\varepsilon_n<10^{-5}$ m rad, and moderately large charge per bunch $Q\cong 200$ pC. This charge is large enough to clearly observe the photoelectrons over the dark-current background, yet small enough that collective effects on the centroid motion, such as transverse wake fields, can be neglected.

The additional advantage this arrangement offers is that the matrix elements to be measured are most strongly dependent on the ratio γ_f/γ_i and on γ'. The PWT is by nature a high-gradient linac ($\gamma'\leqslant 50\ \mathrm{m}^{-1}$), with moderate length $L=42$ cm, and thus to obtain a large value γ_f/γ_i one needs to inject only a relatively small initial energy $\gamma_i m_e c^2$. This energy cannot, however, be made arbitrarily small due to the constraint that $v_b\cong c$ and a related requirement that the relative energy gain per period of the linac be much smaller than unity, both of which are required in order to guarantee the validity of Eq. (1). Thus the injection energy given by the rf gun (which must in fact produce a relativistic beam due to its extraction dynamics) is nearly ideal for maximizing the ma-

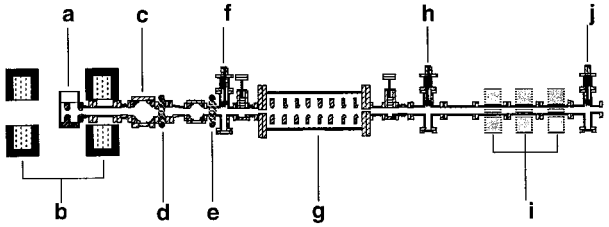

FIG. 1. Layout of the UCLA photoinjector with a (a) 1.5 cell rf gun, (b) focusing and bucking solenoid, (c) mirror box, steering magnets (d) $K1$ and (e) $K2$, (f) phosphor screen $P1$, (g) PWT linac, (h) phosphor screen $P2$, (i) quadrupole triplet, and (j) phosphor screen $P3$.

trix elements given in Eq. (1).

In order to determine the transfer matrix of the PWT linac, the centroid of the photoelectron beam is measured using a differential steering technique originally developed to calibrate the beam energy after the gun. For this measurement, the current I of steering (or kicker) magnet $K1$ is swept while monitoring the centroid position of the electron beam on the downstream phosphor screen $P1$. The image of the beam at the phosphor is obtained with a charge coupled device camera, with the video output recorded by a triggerable digitizing frame grabber. The frame grabber output is further analyzed using on-line software running on a Macintosh personal computer, which also serves to control and read back the steering magnets. The near-axis field integral $\int B_y(I,z)dz$ of the horizontally deflecting steering magnets was determined with Hall probe measurements and the phosphor screens and related video calibrations performed before the experiments. The momentum of the beam is determined from the differential change of the centroid position with current dx_c/dI, by use of the paraxial relation

$$p_0 \cong eL_{11}\frac{dI}{dx_c}\frac{d}{dI}\int B_y dz,$$

with L_{11} equal to the drift length between the center of $K1$ and the first phosphor screen $P1$, and the mean beam momentum in the gun-to-linac section is $p_i=\beta_i\gamma_i m_e c^2 = \sqrt{\gamma_i^2-1}\,m_e c^2$.

This method of momentum determination helps establish the initial conditions of the beam and also forms the technical basis for the matrix element measurements. As it is difficult to determine the actual electromagnetic center of the linac with respect to the insertable phosphor diagnostics, we were forced to use a differential steering technique. In this case, one of the low-energy magnets previous to the linac ($K1$ or $K2$) was swept, while the centroid motion of the beam was observed to be downstream of the linac ($P2$ or $P3$). The four combinations of the steering magnets and observation points, along with knowledge of the drift lengths, integrated field of the steering magnets, and precise calibration of the video images of the phosphor screens, give four measured quantities that allow reconstruction of the linac transport matrix.

For the matrix measurements, the two steering magnets were placed distances of $L_1=44$ cm and $L_2=23$ cm upstream of the linac entrance. The beam profile detection screens $P2$ and $P3$ are located at distances of $L_3=31$ cm and $L_4=96$ cm downstream of the linac. The magnetic flux densities of the three quadrupoles located between the second and third screens were carefully reduced to minimize the perturbing field gradients to a level of 3 G/cm or less, which produces negligible effects on the high-energy beam propagation.

In order to compare these results with the predictions of Eq. (4), we must also measure the energy before (described above) and after the linac. The post-linac energy measurement is performed by use of the spectrometer downstream of $P3$ (not shown in Fig. 1). Once the maximum acceleration for a given amount of rf power directed into the linac is determined with the spectrometer, the phase corresponding to the point $\phi=\pi/2$ and the average accelerating gradient $\gamma' m_e c^2=(E_f-E_i)/L=eE_0$ are established. After this point, the phase of the beam injection relative to the linac can be varied by use of a calibrated phase shifter in the waveguide feed to the linac. The relative power variation to the linac due to the use of the phase shifter is negligible, while use of a waveguide attenuator produces large phase shifts. Thus, if the overall power level fed to the linac is varied (in order to change E_0), then the optimal accelerating phase must be redetermined by the spectrometer energy measurement.

In the initial round of experiments, the dependence of the matrix elements on the linac injection phase was measured. For each phase, we swept through eight different currents in the steering magnets and obtained a linear fit to the resulting centroid motion at the phosphor screens. Three noticeable effects were the source of small errors in this method: (i) a large amount of dark current emitted from the gun, (ii) transverse centroid injection errors arising from cathode drive laser pointing jitter, and (iii) a slow drift in the photocathode drive laser injection phase. This third effect allowed data to be taken over only a limited time span, with all data taken in a single session to ensure the reproducibility of conditions.

The data resulting from these measurements are shown in Fig. 2, which also gives the calculated values of the centroid sweep rate using the transport derived from the M matrix and the relevant drift matrices. There is fairly good agreement for all four measurement sets between the predictions and data over all phases where reliable measurements could be made, with a slightly larger sensitivity on phase offsets from the crest displayed by the data. Note also the larger error bars associated with two measurements made at screen $P3$ shown in Figs. 2(c) and 2(d) for phases of $-2.2°$ and $+10°$. The $P3$ data were inherently more difficult to obtain because the photoelectron beam was much larger in size than at $P2$ and the two more uncertain points suffered from large interference from the dark current background at their specific running conditions.

In order to establish the importance of the rf focusing in these measurements, we have also plotted the predictions derived from matrix transformations obtained in the limit $\eta\rightarrow 0$ in Fig. 2. It can be seen that the agreement with the data is quite poor if the focusing component of the transformation is ignored, establishing the importance of the focusing effects.

The data shown in Fig. 2 can also be inverted to give the elements of the M matrix, with the results shown in Fig. 3. The relative experimental uncertainty shown by the error bars is larger than for the data sets due to the higher-order sensitivity introduced by the inversion process. Also shown in Fig. 3 are the theoretical predictions for the M matrix. Since the matrix elements were more sensitive to the experimental noise in the data, we also fit the data to a quadratic in ϕ and then used the resulting filtered data function in the inversion routine to generate a smooth fit in ϕ for the matrix elements. As can be seen, this fit agrees quite well with theoretical predictions.

As a final check on the validity of these data sets and to independently verify the adiabatic damping component of the transformation, in Fig. 4 we display the experimentally derived values of $\det(M)$ as well as the predicted values γ_i/γ_f. Because of the form of the algebraic relation between the determinant and the matrix elements, the relative experi-

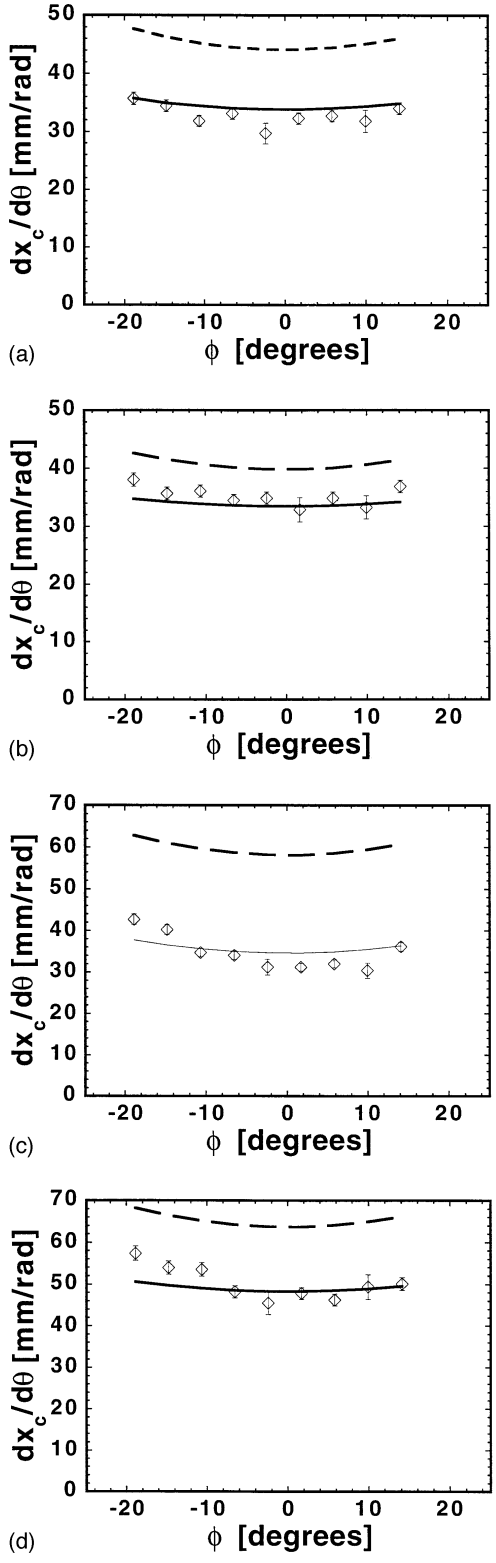

FIG. 2. (a) Centroid motion $dx_c/d\theta$ due to steering magnet $K1$ measured on phosphor screen $P2$, (b) centroid motion $dx_c/d\theta$ due to steering magnet $K1$ measured on phosphor screen $P3$, (c) centroid motion $dx_c/d\theta$ due to steering magnet $K2$ measured on phosphor screen $P2$, and (d) centroid motion $dx_c/d\theta$ due to steering magnet $K2$ measured on phosphor screen $P3$, for different acceleration phases ϕ. Data obtained are marked by diamonds, with predictions from the matrix shown in Eq. (4) given by the solid line and the dashed line showing predictions if focusing effects are ignored (by the limit $\eta \rightarrow 0$) in the matrix.

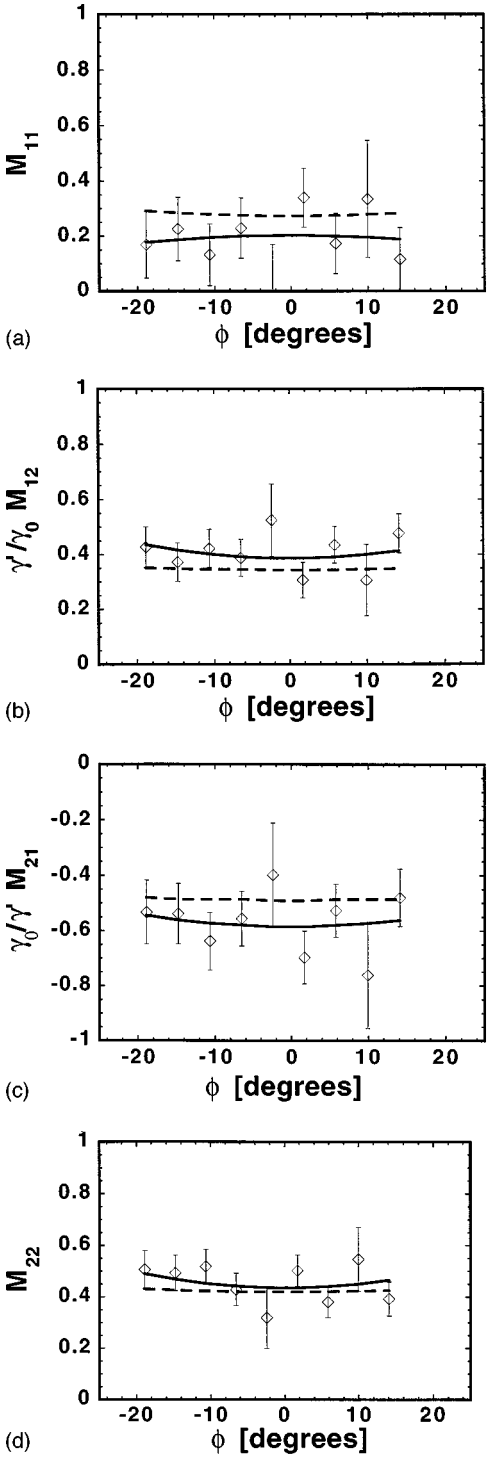

FIG. 3. Matrix elements of the transverse trace space map of the PWT linac: (a) M_{11}, (b) M_{12}, (c) M_{21}, and (d) M_{22}, as a function of phase ϕ. The values obtained from inverting a quadratic fit to the raw data are drawn by a solid line and the theoretical values by a dashed line. The matrix elements M_{12} and M_{21} are weighted by the factors γ'/γ_0 and γ_0/γ', respectively, to normalize all matrix elements.

mental uncertainty in det(M) is no larger than for the elements themselves. We have also plotted the values of det(M) obtained from the quadratic fit to the raw data. Not too surprisingly, this produces agreement with theory as consistent as the agreement found for the matrix elements.

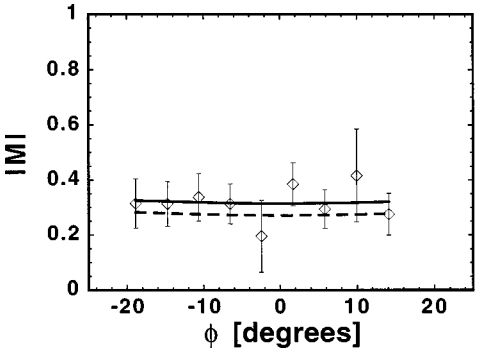

FIG. 4. Determinant of the transverse trace space map for different acceleration phases ϕ. The values for the inverted fit to the data are represented by the solid line and for the theoretical predictions by the dashed line.

In order to complete a parametric study of the predictions of Eq. (4) and explore the adiabatic damping effects in more detail, we undertook a set of measurements of the matrix elements' dependence on E_0. In this case the rf attenuator was used to lessen the power fed into the linac, yielding, after resetting the phase to optimal acceleration, final beam energies of 7.1, 8.7, 10.6, and 12.8 MeV or average accelerating fields of $E_0=8.3$, 12.1, 16.6, and 21.9 MV/m, respectively. The raw data for the beam sweeping measurements are shown in this case in Fig. 5, along with the predictions derived from Eq. (4). Agreement a bit worse in quality than that found in the phase variation case is obtained for this range of accelerating fields. These data can then be inverted as before to give the matrix elements. These experimentally derived determinants are plotted in Fig. 6, along with the predicted values of γ_f/γ_i. This plot, which shows the expected behavior quite well, is taken along with Fig. 4, convincing direct evidence for the adiabatic damping of transverse ''action,'' or area, in trace space.

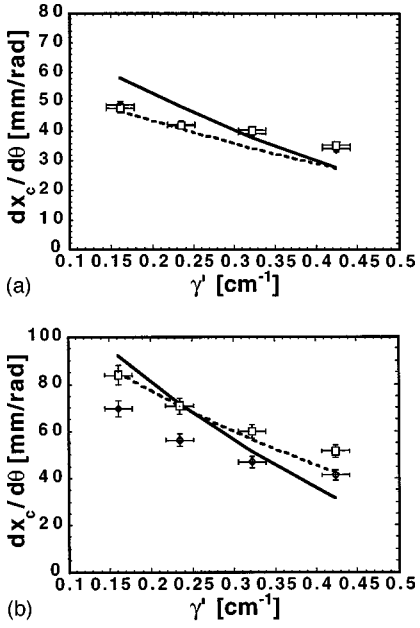

FIG. 5. Centroid motion $dx_c/d\theta$ on (a) phosphor screen $P2$ and (b) phosphor screen $P3$ as a function of acceleration gradients γ'. Data obtained using steering magnet $K1$ are marked by diamonds, with the theoretical predictions for this case given by the solid line; the data from $K2$ are designated by boxes, with dashed line showing predictions.

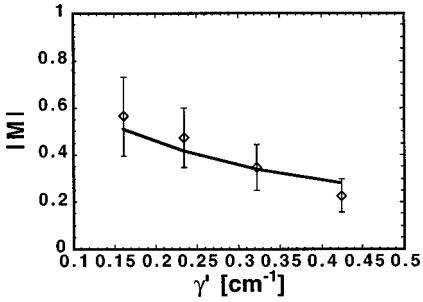

FIG. 6. Determinant of the transverse space map for different acceleration gradients γ'. The theoretical predictions are represented by the solid line.

In conclusion, these sets of measurements have provided verification of the theoretical model developed in Refs. [5,6] of linear transverse dynamics of electrons undergoing simultaneous strong acceleration as well as first- and second-order transverse focusing in a rf linac. The matrix treatment of the dynamics predicted by this model has been directly tested, with the experimentally derived matrix elements in fairly close agreement with the model derived elements. The determinants of the matrices obtained in this manner have been shown to display the expected dependence $\det(M)=\gamma_i/\gamma_f$, giving direct evidence for the adiabatic damping of trace space area.

Some deviations from theoretically predicted matrix elements themselves were noticeable, however, especially in the data obtained at lower acceleration gradient. This artifact, as well as the slightly larger than expected phase dependence of the focusing effects, may be due to the beam excursions in the linac not being small compared to the iris apertures. These excursions would be larger for the cases of smaller acceleration gradient and for off-crest phases, as in both instances the first-order focusing kick encountered by the electrons at the linac entrance would be smaller. In these cases the focusing due to the nonsynchronous spatial harmonics, which is linear only in lowest order, having a modified Bessel function form

$$F_r \sim -\sum_{n=-\infty}^{\infty} b_n I_1(\sqrt{2n(n-1)}k_0 r)/\sqrt{2n(n-1)}k_0$$

(for ultrarelativistic velocities), grows quickly as a function of radial displacement. Evidence that the focusing is generally enhanced in this way can be seen in Fig. 2(c), which shows the ''focusing kick'' element M_{21}; the focusing appears slightly stronger than that expected from linear theory. The phase dependence of the data shown in Figs. 2 and 3 is not only stronger than expected, but also show a slight asymmetry about $\phi=0$, which is also not anticipated from Eq. (4). This is likely due to small phase-dependent $[F_r \sim \sin(\phi)]$ focusing arising from the speed-of-light space harmonic, which is ignored in the approximation $v_b \cong c$ as it gives a net force proportional to γ^{-2} but can be estimated [5] to maximally change the focusing strength by 5% at the injection energy for the phases measured.

The quantitative verification of rf focusing effects establishes the experimental basis for an important theoretical component of many beam optic calculations of contemporary interest. Among these calculations, notable applications include the optics of the TESLA Test Facility [2], a linear collider test accelerator based on superconducting rf standing wave cavities that are to be run at a maximum field strength similar to the present experimental values, as well as a recently developed theory of space-charge dominated beam emittance oscillations in rf photoinjectors [7]. This theory, which relies on the validity of this rf focusing model as one of its crucial assumptions, was developed to understand the emittance compensation process [10], a technique critical to achieving the beam qualities needed for such applications as the x-ray self-amplified spontaneous emission free-electron laser [11]. Finally, proposed future ultrashort-wavelength (perhaps laser-based) accelerators may depend on this type of rf focusing effect to allow the passage of beams through very small apertures [12].

This work was performed with partial support from U.S. Department of Energy, Grants Nos. DE-FG03-90ER40796 and DE-FG03-92ER40693; the Sloan Foundation, Grant No. BR-3225; and the Deutscher Akademischer Austauschdienst (German academic exchange program).

[1] K. J. Kim, Nucl. Instrum. Methods Phys. Res. A **275**, 201 (1989).

[2] TESLA Test Facility Linac-Design Report, DESY TESLA Report No. 95-01 (DESY, Hamburg, 1995).

[3] E. Chambers (unpublished).

[4] R. Helm and R. Miller, in *Linear Accelerators*, edited by Pierre M. Lapostolle and Albert L. Septier (North-Holland, Amsterdam, 1969).

[5] S. C. Hartman and J. B. Rosenzweig, Phys. Rev. E **47**, 2031 (1993).

[6] J. Rosenzweig and L. Serafini, Phys. Rev. E **49**, 1599 (1994). Note the correction in our Eq. (4) of a typographical error in the expression for M_{21} in this paper.

[7] L. Serafini and J. Rosenzweig, Phys. Rev. E **55**, 7565 (1997).

[8] R. Zhang *et al.*, in *Proceedings of the 1995 Particle Accelerator Conference*, edited by D. Rusthoi (IEEE, Piscataway, NJ, 1995), p. 1102; D. Swenson, in *Proceedings of the 1988 European Particle Accelerator Conference*, edited by S. Tazzari (World Scientific, Singapore, 1989).

[9] U. Happek, A. J. Sievers, and E. B. Blum, Phys. Rev. Lett. **67**, 2962 (1991).

[10] B. E. Carlsten, Nucl. Instrum. Methods Phys. Res. A **285**, 313 (1989).

[11] C. Pellegrini *et al.*, Nucl. Instrum. Methods Phys. Res. A **331**, 223 (1993).

[12] J. Rosenzweig *et al.*, Phys. Rev. Lett. **74**, 2467 (1995).